

# Multiplicity, transverse momentum and pseudorapidity dependence of open-heavy flavored hadron production in proton+proton collisions at $\sqrt{s}=13$ TeV

Bhagyarathi Sahoo, Suman Deb, and Raghunath Sahoo\*

*Department of Physics, Indian Institute of Technology Indore, Simrol, Indore 453552, India*

(Dated: August 24, 2022)

Recently, with the upgradation of LHC, it is realized that study of heavy-flavored hadrons, namely  $\Lambda_c^+$  and  $D^0$  in hadronic collisions, could reveal the possibility of thermalization of charm quarks. With this motivation, we study the production dynamics of these hadrons in proton+proton collisions at  $\sqrt{s}=13$  TeV by exploiting their dependence on charged-particle multiplicity, transverse momentum, and pseudorapidity using a pQCD-inspired model called PYTHIA8. With the help of the established PYTHIA8 tunes to mimic the behavior of thermalization, we investigated the variation of effective temperature and degree of non-extensivity using thermodynamically consistent non-extensive Tsallis statistics. We further attempted to establish a connection between the initial state and final state by estimating the correlation between the number of multi-partonic interactions ( $n_{MPI}$ ) with the Knudsen number.

PACS numbers:

## I. INTRODUCTION

Heavy-flavor quarks (charm and beauty) are mostly produced in the early stages of ultra-relativistic high-energy hadronic and nuclear collisions by hard parton-parton scattering processes. These processes predominantly include production of heavy-flavor quarks through gluon fusion ( $gg \rightarrow c\bar{c}/b\bar{b}$ ) and quark-antiquark annihilation ( $q\bar{q} \rightarrow c\bar{c}/b\bar{b}$ ). The hadrons formed from these quarks, both hidden and open, charmed and beauty flavors are considered a vital probe to understand the dynamics of systems formed in both the hadronic and nucleus-nucleus collisions. Starting from their suppression in heavy-ion collisions (HIC) to comprehending production mechanism in proton+proton (pp) collisions through understanding cold nuclear effect (CNM) in proton on lead collisions, heavy flavored hadrons play a major role. Moreover, because of their heavy mass and larger relaxation time compared to the lifetime of quark-gluon plasma (QGP), a deconfined equilibrated state of quarks and gluons, they experience the entire phase-space evolution process and consequently carry information about the medium. In recent times, both experimental results like strangeness enhancement [1], ridge-structure [2, 3], etc., and theoretical results [4, 5] of pp collisions have brought a wave of excitement to the particle physics community, which are conventionally considered as heavy-ion-like QGP signatures. These results compel us to reinvestigate the traditional understanding of using pp collisions as a benchmark to study the formation of a QGP medium in HIC. In this context of better understanding the dynamics of pp collisions, heavy-flavored hadrons are believed to be one of the best tools. This is because their dynamics differ from the light flavored hadrons, as heavy quarks are formed

mostly by the perturbative hard-Quantum Chromodynamics (pQCD) processes in contrast to the light quarks, which are produced by non-perturbative Quantum Chromodynamic processes.

Various phenomenological models [6–8] attempt to explain the behavior of relative  $J/\psi$  yield as a function of relative charged-particle multiplicity measured in pp collision at  $\sqrt{s}=13$  TeV in ALICE experiment at the LHC [9, 10]. One of these phenomenological models is PYTHIA8, a pQCD-inspired model that could be used to study the dynamics of heavy-flavored production in small systems concerning the LHC energies. It is seen that PYTHIA8, with the help of its tunes, namely multi-parton interactions (MPIs) and color reconnection (CR), could mimic the behaviour of thermalization [11]. This feature of PYTHIA8 has been exploited in literature to study the thermodynamical quantities in pp collisions [12, 13]. To have a comprehensive prospect on the dynamics of heavy flavored baryon and meson, in the present work, we have also used these features of PYTHIA8 to perform a transverse momentum ( $p_T$ ) - a differential study of  $\Lambda_c^+$  and  $D^0$ . It is worth recalling here that the possibility of thermalization in small systems was in fact studied in 1953 by Landau in the context of collisions of small systems [14–17]. This shows the importance of the subject matter and its implications for the LHC energies.

The statistical approach gives a better description of dealing with a complex system formed in the hadronic and nuclear collisions. The study of final state transverse momentum spectra dispenses knowledge about the kinetic freeze-out processes in such collisions. With this motivation, we have analyzed the  $p_T$ -spectra of  $\Lambda_c^+$  and  $D^0$  to extract thermodynamic information in a wide  $p_T$ -range using a thermodynamically consistent non-extensive distribution function, called the Tsallis distribution [18–23]. This distribution function explains the transverse momentum spectra of final state particles in both hadronic and HIC collisions at a larger  $p_T$ -

---

\*Corresponding author email: Raghunath.Sahoo@cern.ch

range very well while taking care of both the aspects of particle production, namely, the pQCD-based and non-pQCD-based processes. Further, it contains two important parameters: effective temperature (T) or Tsallis temperature and non-extensive parameter (q). This non-extensive parameter indicates the degree of deviation of the system from an equilibrium state, which is correlated with the Tsallis temperature. The effective temperature doesn't give the full picture of the particle production dynamics at the freeze-out due to the finite or rather significant contribution from the radial flow-effects [21, 24]. Thus, in this work, we have studied the kinetic freeze-out temperature ( $T_{kfo}$ ) using  $\Lambda_c^+$  and  $D^0$  in the pp system. Since charged-particle multiplicity is a good replacement for centrality in the pp system and acts as a proxy for the number of constituents formed in a system after the collision, we have studied the freeze-out scenario with charged-particle multiplicity. Through various studies [25, 26], it is understood that different regions of  $p_T$ -spectra could shed more light on the origin of particle hadronization while traversing through the medium. With this in mind, we have also investigated the variation of freeze-out scenarios with transverse momentum spectra. Further, in the HIC, since the midrapidity regions are mostly dominated by gluons while forward rapidity by the constituent quarks, it is interesting to study the rapidity dependence of particle production, which is explored here.

One of the purposes of the present work is to study the thermalization effect on heavy-flavored hadrons, viz.,  $\Lambda_c^+$  and  $D^0$  in pp collisions by calculating some of the thermodynamical quantities like the squared speed of sound ( $c_s^2$ ), isothermal compressibility ( $\kappa_T$ ) and the Knudsen number ( $K_n$ ). The squared speed of the sound describes the interaction strength of the particles in a medium. While isothermal compressibility describes the compression nature of the medium, the Knudsen number describes the hydrodynamical behavior of the system. The fluctuation in Tsallis temperature is related to the non-extensive parameter (q) [27] and both these parameters are particle species dependent [21]. In this regard, we have analyzed the statistical correlation between T and q to investigate their dependence on the mass of the particle. Since we are using PYTHIA8 for the present work, we have access to the mean number of multi-partonic interactions ( $\langle n_{MPI} \rangle$ ), which gives information on the interaction at the partonic level. The calculation of the inverse of the Knudsen number at the hadronic-phase boundary provides information on the number of hadronic interactions at the phase boundary. It would be interesting to understand the correlation dynamics between these two numbers, as they connect the initial state with the final state of the system. Heavy-flavored baryons and mesons could be a better probe as they witness the whole system's space-time evolution.

This paper is organized as follows. After the introduction and definition of the physics problem in hand, in the present section I, we move forward in giving a brief de-

tail of event generation using PYTHIA8 and the analysis methodology in section II. Section III includes the results obtained from the analysis of  $p_T$ -spectra for  $\Lambda_c^+$  and  $D^0$  in pp collisions. Finally, we conclude with a summary of the important findings in section IV.

## II. EVENT GENERATION AND ANALYSIS METHODOLOGY

### A. Event Generation

Event Generators are the most effective substitutes for realistic experiments involving the hadronic and nucleus-nucleus collisions (AA). These generators are based on the Monte Carlo techniques for simulating the collisions using physics processes to better understand the nature of the events. Based on the kind of colliding species involved and underlying known physics processes, there are several event generators like AMPT [28] (for nucleus-nucleus collisions), PYTHIA (for both pp and AA collisions), EPOS LHC [29] (for hadronic and nuclear collisions), etc. Among them, PYTHIA is one of the widely used event generators for simulating ultra-relativistic collisions among particles like electron-electron, electron-positron, proton-proton, and proton-antiproton. It is highly successful in explaining many experimental results at the LHC. PYTHIA involves many physics mechanisms like hard and soft interactions, parton distributions, initial and final state parton showers, multipartonic interactions, string fragmentation, color reconnection and resonance decays, rescattering, and beam remnants [30].

In this study, we have used PYTHIA 8.235 to generate pp collisions at  $\sqrt{s} = 13$  TeV with 4C Tune (Tune:pp = 5) [31]. Subsequent Multi-Partonic Interaction (MPI) process is one of the main advantages of PYTHIA 8.235 over PYTHIA6 along with invariant parameter dependence of collision, which allows heavy-flavor quarks production through  $2 \rightarrow 2$  hard subprocesses. A detailed explanation of all physics processes involved in PYTHIA 8.235 can be found in Ref. [32].

For our study, we contemplate inelastic, non-diffractive simulated events. So in the total scattering cross section, only the non-diffractive component of all hard QCD processes (HardQCD:all=on) will contribute. Hard processes involve the production of heavy quarks. We have considered mode two of color reconnection (ColourReconnection:mode = 2) along with MPI (PartonLevel:MPI = on). The data are simulated considering color reconnection on (ColourReconnection:reconnect = on) and color reconnection off (ColourReconnection:reconnect = off). To avoid the divergences of QCD processes in the limit  $p_T \rightarrow 0$  a transverse momentum cut of  $p_T \geq 0.5$  GeV/c (PhaseSpace:pTHatMinDiverge = 0.5) is taken. For the production of  $\Lambda_c^+$  and  $D^0$ , we use Charmonium:all flag (Charmonium:all = on) in the simulation [33–35] through NRQCD framework. Study of  $\Lambda_c^+$  and  $D^0$  are done at mid and forward rapidities.  $\Lambda_c^+$  ( $D^0$ ) decays via

$p + K^- + \pi^+$  [36] ( $K^- + \pi^+$  [37]) because of high branching ratio of these modes. This analysis is performed by generating 120 million events in pp collisions at  $\sqrt{s} = 13$  TeV for all the rapidities discussed here.

To check the compatibility of PYTHIA8 with experimental data, we have used the same tuning as used in one of our previous works described in Ref [38], where we have compared the experimental data with PYTHIA8 simulated data for  $D^0$ . Because of the unavailability of experimental  $p_T$ -spectra of  $\Lambda_c^+$  for pp collisions at  $\sqrt{s} = 13$  TeV at the time of this work, we could not compare our results with experimental data.

## B. Analysis Methodology

The  $p_T$ -spectra of produced particles usually follow the thermalized Boltzmann type of distribution, given as

$$E \frac{d^3 N}{dp^3} \simeq C \exp\left(\frac{-p_T}{T_{kin}}\right), \quad (1)$$

where  $C$  is the normalization constant and  $T_{kin}$  is the kinetic freeze-out temperature. It is observed that at LHC/RHIC, the low- $p_T$  part ( $< 3$  GeV/c) is well explained by the Boltzmann-Gibbs Blast Wave model taking radial flow into account, but the high- $p_T$  spectra do not follow Boltzmann type distribution. This could be because of possible pQCD processes, which have a power-law contribution to the spectra.

To explain the whole range of  $p_T$ -spectra, one has to take care of the power law contribution at high- $p_T$  [39–41]. Hagedorn proposed an empirical formula to describe the whole  $p_T$  range, in which high- $p_T$  region follows a power-law function, while the low- $p_T$  follows an exponential function [42]. A similar kind of observation also can be found with the thermodynamically consistent form of the Tsallis distribution function having a functional form, given by:

$$f(E) \equiv \exp_q\left(-\frac{E - \mu}{T}\right), \quad (2)$$

where  $E = \sqrt{p^2 + m^2}$  is the energy of the particle, and  $\mu$  is the chemical potential of the system.

The  $\exp_q(x)$  has the following form:

$$\exp_q(x) \equiv \begin{cases} [1 + (q-1)x]^{\frac{1}{q-1}} & \text{if } x > 0 \\ [1 + (1-q)x]^{\frac{1}{1-q}} & \text{if } x \leq 0 \end{cases} \quad (3)$$

where  $x = \frac{E - \mu}{T}$ . In the limit,  $q \rightarrow 1$ , Eq. 3 reduces to an exponential function.

$$\lim_{q \rightarrow 1} \exp_q(x) \rightarrow \exp(x) \quad (4)$$

Consequently, the invariant yield in terms of Eq. 2 could be expressed as

$$E \frac{d^3 N}{dp^3} = gV E \frac{1}{(2\pi)^3} [1 + (q-1) \frac{(E - \mu)}{T}]^{\frac{-q}{q-1}} \quad (5)$$

where  $g$  is the degeneracy factor,  $V$  is the volume of the system.

In terms of rapidity ( $y$ ), transverse mass ( $m_T$ ), and transverse momentum ( $p_T$ ), Eq. 5 becomes

$$\frac{d^2 N}{dp_T dy} = gV \frac{p_T m_T \cosh y}{(2\pi)^2} [1 + (q-1) \frac{(m_T \cosh y - \mu)}{T}]^{\frac{-q}{q-1}} \quad (6)$$

where,  $m_T = \sqrt{p_T^2 + m^2}$  is the transverse mass.

At LHC energies, chemical potential is assumed to be nearly zero ( $\mu \simeq 0$ ) and at midrapidity ( $y=0$ ), Eq. 6 reduces to :

$$\frac{d^2 N}{dp_T dy} = gV \frac{p_T m_T}{(2\pi)^2} [1 + (q-1) \frac{m_T}{T}]^{\frac{-q}{q-1}} \quad (7)$$

The thermodynamic quantities like number density ( $n$ ), energy density ( $\epsilon$ ), and pressure ( $P$ ) can also be calculated in terms of the Tsallis distribution function to search for the thermal behavior of the discussed particles in each multiplicity class. These quantities as expressed as follows,

$$n = g \int \frac{d^3 p}{(2\pi)^3} f^q \quad (8)$$

$$\epsilon = g \int \frac{d^3 p}{(2\pi)^3} E f^q \quad (9)$$

$$P = g \int \frac{d^3 p}{(2\pi)^3} \frac{p^2}{3E} f^q \quad (10)$$

By using the above thermodynamic quantities, one can obtain the crucial indicators of thermalization like the speed of sound ( $c_s$ ), isothermal compressibility ( $\kappa_T$ ), and Knudsen number ( $K_n$ ), which are of interest for the present work.

The squared speed of sound is defined as the change in pressure of the system with respect to a change in the energy density at constant entropy density and number density. Mathematically,

$$c_s^2 = \left(\frac{\partial P}{\partial \epsilon}\right)_{s,n} \quad (11)$$

It describes the hydrodynamical evolution and equation of the state of the thermal medium. It helps us

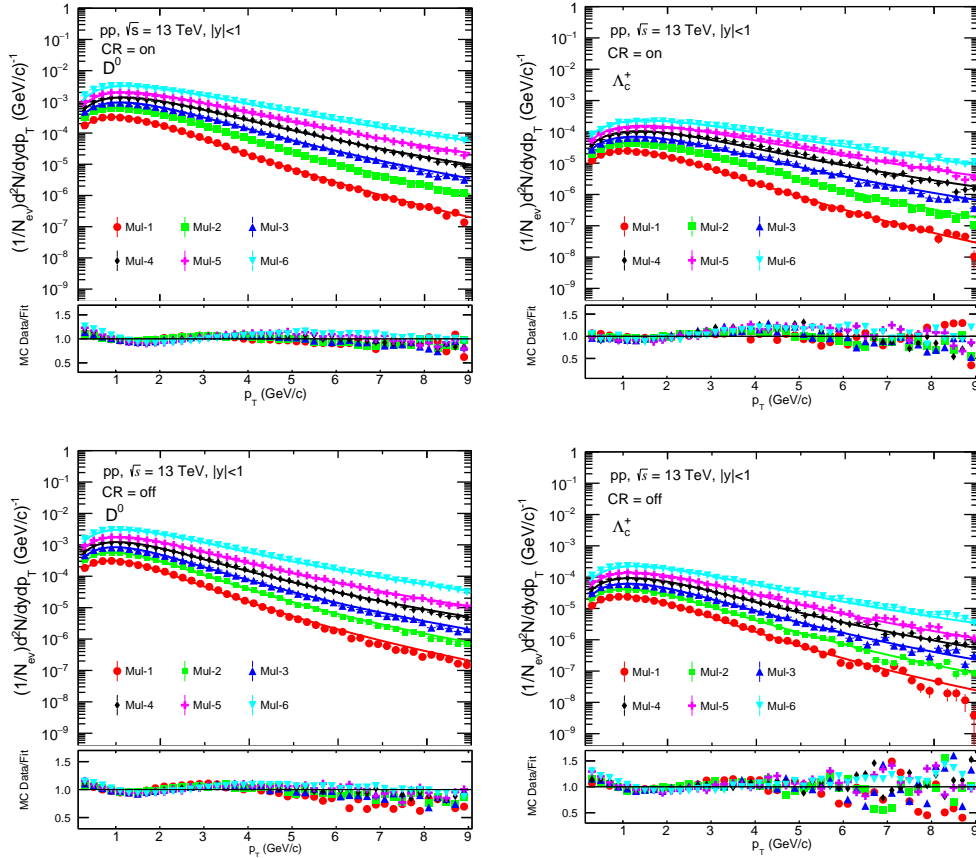


FIG. 1: (Color online) Upper (lower) panel shows the fitting of simulated  $p_T$ -spectra of  $\Lambda_c^+$  and  $D^0$  from PYTHIA8 using Tsallis distribution function for CR = on (CR = off) in different multiplicity classes as shown in Table I.

to characterize the interaction strength of the QCD medium formed after the collision, i.e., whether it is strongly interacting or not or how much it differs from the ideal massless non-interacting gas. It is inversely proportional to the compressibility of the fluid.

The isothermal compressibility ( $\kappa_T$ ) is defined as the change in volume of the system with a change in pressure at a constant temperature.

$$\kappa_T = -\frac{1}{V} \left( \frac{\partial V}{\partial P} \right)_T \quad (12)$$

It is a response function that defines the compression nature and equation of the state of the medium. The value of isothermal compressibility is very sensitive to charged-particle multiplicity fluctuation, temperature, and volume of the system.

Knudsen number ( $K_n$ ) is defined as the ratio of the mean free path ( $\lambda$ ) of a particle to a spatial dimension of the system ( $R$ ).

$$K_n = \frac{\lambda}{R} \quad (13)$$

It defines the hydrodynamic behavior of the system. When the Knudsen number,  $K_n \gg 1$ , this indicates that the system is far from thermodynamic equilibrium and a smaller value of the Knudsen number, tending to zero, indicates that the system has higher degrees of thermalization and follows a hydrodynamic behaviour.

With the brief introduction to the methodology and all the quantities involved in the present analysis, we now move toward the results and discussion section.

### III. RESULTS AND DISCUSSION

In this section, we discuss the results in three consecutive subsections. Firstly, in subsection III A, we discuss the behavior of Tsallis extracted effective temperature and non-extensive parameter ( $q$ ) as a function of charged-particle multiplicity, transverse momentum, and pseudo-rapidity. This effective temperature contains a contribution from both kinetic freeze-out temperature and transverse radial flow. Secondly, in subsection III B, to have information about the behavior of kinetic freeze-out temperature and the contribution of radial flow to the effec-

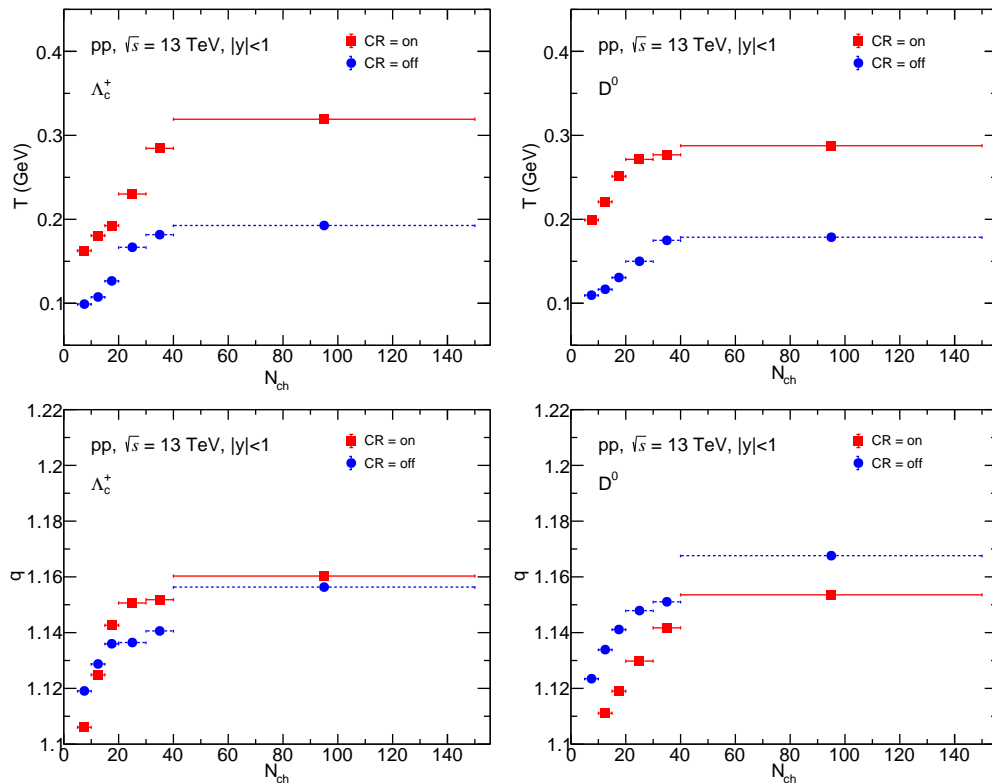


FIG. 2: (Color online) Upper and lower panels show the Tsallis extracted parameters,  $T$  and  $q$  with charged-particle multiplicity, respectively by considering both color reconnection mode on and off, for  $\Lambda_c^+$  and  $D^0$ .

tive temperature, we make a thermodynamic study considering only the high/close to high-multiplicity events. Thirdly, in subsection III C, we make a correlation study between different Tsallis thermodynamic parameters.

### A. Transverse momentum spectra and Non-extensivity

The  $p_T$ -spectra of  $\Lambda_c^+$  and  $D^0$  obtained from the PYTHIA simulation of  $pp$  collision at  $\sqrt{s} = 13$  TeV are fitted with the non-extensive statistical distribution function and are shown in Fig. 1. The deviation of the fitting function from transverse momentum spectra of both  $\Lambda_c^+$  and  $D^0$  are shown in the bottom panels. The fitting parameter, viz., effective temperature ( $T$ ), and non-extensive parameter ( $q$ ), obtained as a function of charged-particle multiplicity along with the goodness of the fit in terms of  $\chi^2/ndof$  is given in Table II. The charged-particle multiplicity classes used in the present analysis are taken from Ref [38] and are shown in Table. I.

From the spectra, it is clearly observed that the particle production mechanism is different at different  $p_T$  regions ( for instance,  $p_T < 3$  GeV/c and above). From the ratio between MC simulated data points with the fit function, it is observed that non-extensive statistics provide a

good description for open heavy flavor transverse momentum spectra for a broader  $p_T$  range. The fitting function fits well with simulated data points within uncertainties for the entire  $p_T$  range, ensuring the correctness of fitting. In the context of multiplicity classes, we observed that the Tsallis function explains high-multiplicity classes relatively better than low-multiplicity classes at the high- $p_T$  range. This could perhaps be the artifact of the choice of fitting range. We also observed the effect of color reconnection on open charm hadrons production dynamics using the tuning feature of PYTHIA8. The dependence of fitting parameters  $T$  and  $q$  with charged-particle multiplicity, transverse momentum, and pseudorapidity are studied separately.

Figure 2 shows that the extracted effective temperature ( $T$ ) and the non-extensive parameter ( $q$ ) increase with charged-particle multiplicity class ( $N_{ch}$ ) both for  $\Lambda_c^+$  and  $D^0$ . This increase is observed for both presence and absence of the color reconnection mode of hadronization. The increasing trend of effective temperature with charged-particle multiplicity indicates that at high-multiplicity, heavy flavor particles ( here  $\Lambda_c^+$  and  $D^0$  ) freeze out earlier in time as compared to the low-multiplicity class of events. Interestingly, it is observed that the effective temperature is less in color reconnection mode off as compared to the color reconnection mode

TABLE I: Charged-particle multiplicity classes ( $N_{ch}$ ) ( $|\eta| < 0.8$ ) corresponding to different events

MultiplicityClass	Mul-1	Mul-2	Mul-3	Mul-4	Mul-5	Mul-6
$N_{ch}$	5-10	10-15	15-20	20-30	30-40	40-150

TABLE II: The extracted Tsallis parameters as well as the  $\chi^2/\text{ndf}$  for all the multiplicity classes both for  $\Lambda^+$  and  $D^0$ 

Particles		Multiplicity class					
		Mul1	Mul2	Mul3	Mul4	Mul5	Mul6
$\Lambda_c^+(\text{CR} = \text{on})$	T (GeV)	0.1626±0.0004	0.1806±0.0004	0.1925±0.0005	0.2302±0.0005	0.2846±0.0007	0.3192±0.0008
	q	1.1060±0.0005	1.1249±0.0005	1.1426±0.0006	1.1506±0.0006	1.1518±0.0008	1.1603±0.0008
	$\chi^2/\text{ndf}$	3.0093	4.9144	8.1237	12.4347	8.3017	5.8085
$\Lambda_c^+(\text{CR} = \text{off})$	T (GeV)	0.9904± 0.0003	0.1075± 0.0004	0.1266±0.0005	0.1667±0.0005	0.1817±0.0006	0.1927±0.0004
	q	1.1191±0.0005	1.1288±0.0006	1.1360±0.0008	1.1364±0.0007	1.1406±0.0008	1.1563±0.0006
	$\chi^2/\text{ndf}$	5.7099	4.6264	3.5093	4.5320	5.5214	9.5009
$D^0(\text{CR} = \text{on})$	T (GeV)	0.1992±0.0014	0.2208±0.0014	0.2511±0.0019	0.2714±0.0017	0.2768±0.0019	0.2876±0.0001
	q	1.0996±0.0005	1.1111±0.005	1.1190±0.0006	1.1298±0.0005	1.1417±0.0006	1.1536±0.0002
	$\chi^2/\text{ndf}$	21.3212	22.5797	26.4923	23.8971	21.1096	29.3412
$D^0(\text{CR} = \text{off})$	T (GeV)	0.1096±0.0001	0.1167±0.0037	0.1307±0.0028	0.1500±0.0030	0.1750±0.0034	0.1787±0.0001
	q	1.1235±0.0002	1.1339±0.0014	1.1411±0.0010	1.1479±0.0010	1.1511±0.0011	1.1676±0.0002
	$\chi^2/\text{ndf}$	16.3096	10.2263	8.5988	12.9793	10.9633	22.1292

on for all multiplicity classes. This could be due to the fact that CR along with MPIs could mimic the thermalization effect, and the absence of either of them in the simulation process is picked up by the decrease in effective temperature. CR being a hadronization process, it increases the number of particles in the system and along with MPI, it helps the system to thermalize. However, it is observed that the effective temperature is lower for the CR off case, as compared to the CR on case, which goes in line with the observation that the  $p_T$ -spectra in CR off cases are harder than the CR on cases. When CR is off, the pQCD processes stay in the system making the system temperature lower than the case of CR on cases. The higher value of q with charged-particle multiplicity indicates that the particle is away from equilibrium in all multiplicity classes. Since  $\Lambda_c^+$  and  $D^0$  are heavy particles, their production dynamics are different compared to light flavor particles studied in Ref. [21, 26]. The chances of equilibrium in the medium are very low for heavy-flavored particles.

Next, we attempted to study the behavior of T and q with transverse momentum ( $p_T$ ), considering only the lowest and highest multiplicity classes. This is done by slicing the  $p_T$ -spectra in steps of 0.4 GeV/c and fitting each slice by the Tsallis distribution function, which is followed by extraction of fitting parameters. This study serves a dual purpose viz., because of the different number densities, the environment at low and high-multiplicity classes will be very different from each other and because of different particle production mechanisms at different  $p_T$  regions. From fig. 3, it is observed that the effective temperature as a function of  $p_T$  shows a decreasing trend with increase in  $p_T$  for the low-multiplicity classes. And for high-multiplicity classes, this trend seems to get reversed. This observation matches the results found in Ref [26], where a similar analysis was per-

formed by considering only final state charged-particles. This could be comprehended from the particle  $p_T$ -spectra evolution with multiplicity classes as shown in fig. 1, where it is observed that the particle production at the low- $p_T$  range for the low-multiplicity classes is more dominated by the thermal contribution as compared to the high-multiplicity classes.

For the non-extensive parameter q in fig. 3, it is observed that it increases with  $p_T$  up to (2-3) GeV/c and then saturates towards high- $p_T$  both for the lowest and highest multiplicity classes. Both  $D^0$  and  $\Lambda_c^+$  were observed to follow the same trend irrespective of the mode of color reconnection. We found a different trend for q as a function of  $p_T$  as compared to Ref. [26]. This could probably be because of the different particle production mechanisms of the heavy-flavored hadrons, which are coming from hard-QCD processes in contrast to the light-flavored hadrons.

We further extend our analysis to study the pseudorapidity ( $\eta$ ) dependence of T and q for the entire  $p_T$  range considering different  $\eta$  bins from 0 to 2.4 in steps of 0.2 covering mid and forward rapidities. This is followed by extracting values of T and q for each  $p_T$ -bin after fitting the spectra with the Tsallis function. This is made possible because PYTHIA8 is quite robust in describing both the low and high- $p_T$  part of the experimental transverse momentum spectra.

Fig. 5 shows the pseudorapidity ( $\eta$ ) dependence of effective temperature (T) and the non-extensive parameter (q). It is observed that the effective temperature decreases with an increase in pseudorapidity ( $\eta$ ). A similar result was found in Ref [43]. This observation of a higher effective temperature at midrapidity is because of the large transfer of energy density in the lower pseudorapidity region, which leads to a very high degree of excitation of the system. This results in a higher T-value

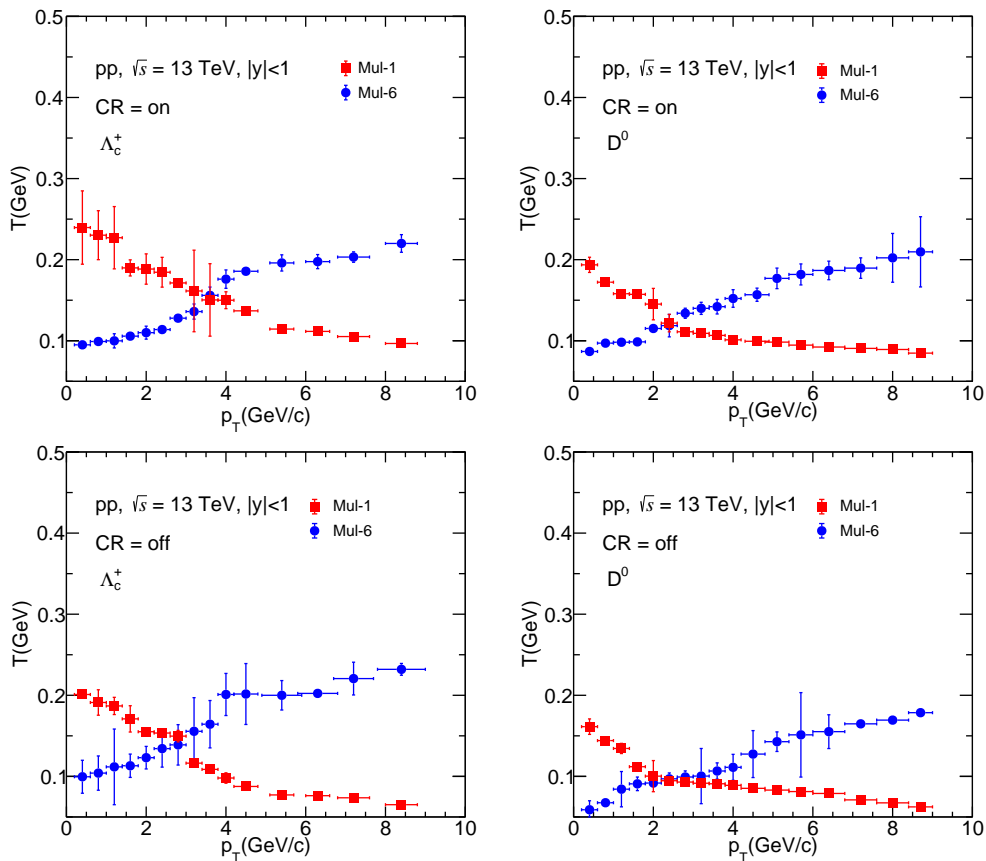


FIG. 3: (Color online) Upper and lower panels show the Tsallis temperature parameters,  $T$  with transverse momentum for  $\Lambda_c^+$  and  $D^0$  by considering both color reconnection mode on and off.

in the lower pseudorapidity region. This also goes in line with a higher number of secondaries being produced at the midrapidity as compared to the forward rapidities. With a higher number of particles at the midrapidity region, it is expected that the system should approach a thermodynamic equilibrium faster than the system usually produced at the forward rapidity. This is also reflected in our results, where we observe the non-extensive parameter ( $q$ ) being closer to unity for the midrapidity region and it goes away from equilibrium when one moves towards the forward rapidities. This is in line with the results reported in Ref. [43].

### B. Multiplicity dependence of $c_s^2$ , $\kappa_T$ and $K_n$

Here, we discuss the variation of thermodynamic quantities like the squared speed of sound ( $c_s^2$ ), isothermal compressibility ( $\kappa_T$ ), the Knudsen number ( $K_n$ ) with charged-particle multiplicity, which is briefly motivated in section II B. Using Tsallis distribution function given by Eq. 2, these thermodynamical quantities are calculated and the final mathematical forms are expressed in Eqs. 11, 12 and 13. The Tsallis parameters, namely,  $T$

and  $q$  obtained as a function of charged-particle multiplicity in the previous section III A are used to compute the above-mentioned thermodynamic quantities for  $\Lambda_c^+$  and  $D^0$ . It is worth noting that the  $(T, q)$  used here are from CR = on mode only as CR with MPI was found to mimic thermalization in a small system, as reported in Ref. [11].

Figure 6 shows the variation of  $c_s^2$ ,  $\kappa_T$  and  $K_n$  with charged-particle multiplicity for  $\Lambda_c^+$  and  $D^0$ . We observed that  $c_s^2$  increases with multiplicity and approaches the ideal gas limit or Stefan-Boltzmann limit ( $1/3$ ), where the particles are assumed to be massless and non-interacting towards the higher multiplicity classes. This observation indicates that the high-multiplicity medium is more thermal-like than the low-multiplicity environment. Since in the present work, we are dealing with heavy flavor particles, which have comparatively higher mass compared to light flavors, it is an interesting observation that the effect of interaction strength is also prevalent in the charm sector. We further observed that the mass ordering in the speed of sound is also preserved in all multiplicity classes, i.e., massive particles ( $\Lambda_c^+$ ) have less  $c_s^2$  value as compared to  $D^0$ , which is relatively less massive. This result agrees with previous findings re-

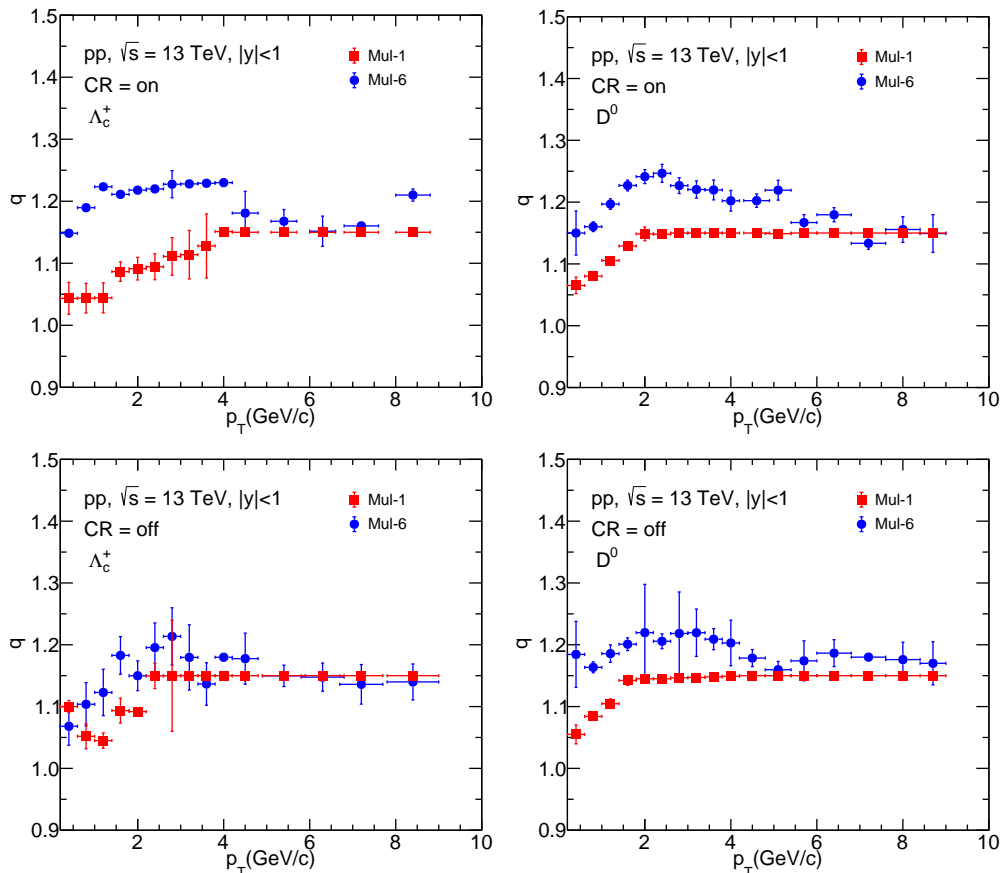


FIG. 4: (Color online) Upper and lower panels show the Tsallis non-extensive parameters,  $q$  with transverse momentum for  $\Lambda_c^+$  and  $D^0$  by considering both color reconnection mode on and off.

ported in Ref. [12]. In the case of  $\kappa_T$ , we observe that it is very sensitive to charged-particle multiplicities in the final state. In lower multiplicity classes, the value of isothermal compressibility is relatively high. It starts to decrease with the increase in particle multiplicity until it attains a minimum value at the higher multiplicity classes. This observation shows that the system is more incompressible at higher multiplicities. This result also agrees with previous findings, as shown in Ref. [44]. Further, the Knudsen number in fig. 6 is observed to decrease with charged-particle multiplicity. Going in accordance with Eq. 13, this decrease is expected only if the system is in thermal equilibrium owing to interaction length being much smaller than system size and a hydrodynamical treatment is applicable. This result of  $K_n$  towards high-multiplicity events somewhat confirms the probability of a high-multiplicity class to be thermally equilibrated as indicated by the observation of  $c_s^2$  and  $\kappa_T$ .

From the above observations, it is clear that the system shows less thermodynamic behavior at low multiplicities as compared to higher multiplicity classes. This inference has compelled us to use a high-multiplicity class to study the kinetic freeze-out scenario, i.e., to extract ki-

netic freeze-out temperature.

The temperature ( $T$ ) arising from non-extensive statistics is a temperature-like parameter, although it obeys the thermodynamic consistency relations. However, it is still not equivalent to the Boltzman-Gibbs temperature, as it also includes the contribution from the mass-dependent flow. The kinetic freeze-out information can be extracted from  $T$ -parameter by using the linear relation:

$$T = T_{kfo} + \frac{1}{2}mv_{flow}^2, \quad (14)$$

where  $T_{kfo}$  is the kinetic freeze-out temperature,  $m$  is the mass of the particle, and  $v_{flow}$  is the collective flow velocity.  $T_{kfo}$  is obtained from the intercept of the fit using Eq. 14 in the plot of  $T$  as a function of  $\Lambda_c^+$  and  $D^0$  mass. We mainly focus on the high-multiplicity region, which behaves more like the thermal medium as discussed above. The value of kinetic freeze-out temperature for the high-multiplicity class is found to be  $T_{kfo} = 0.148 \pm 0.004$  GeV. The value of the kinetic freeze-out temperature at high-multiplicity decreases more rapidly as compared to the effective temperature as shown in ta-



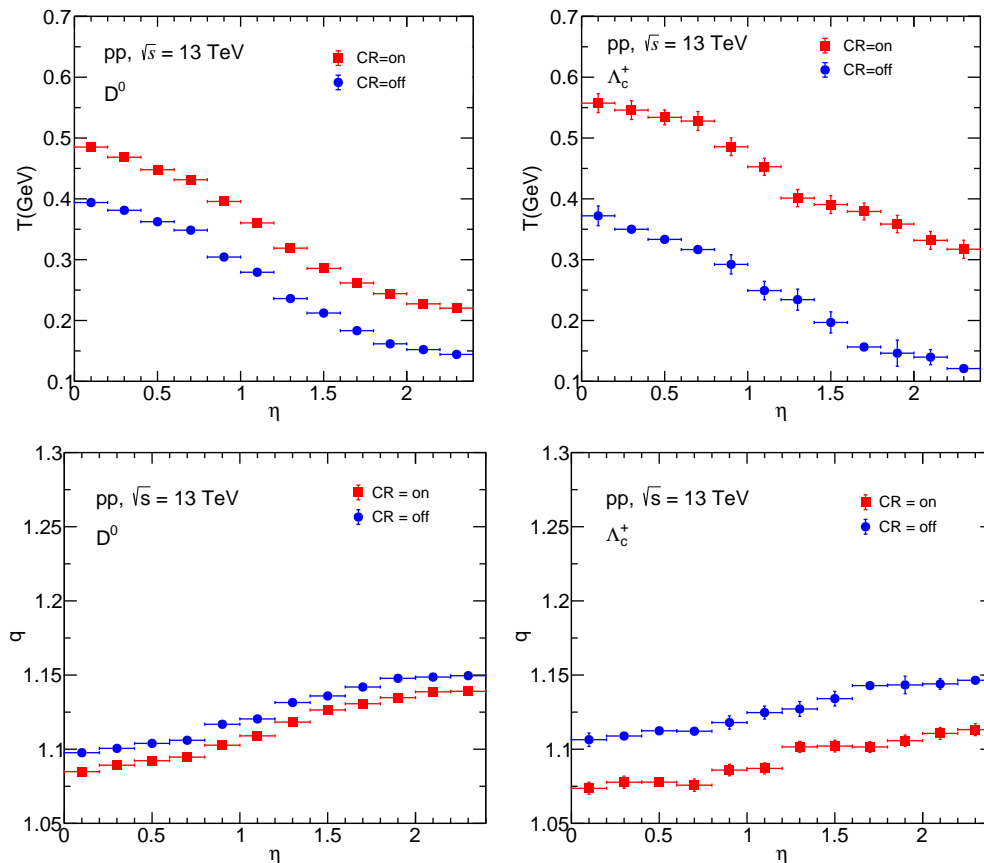


FIG. 5: (Color online) Upper and lower panels show the Tsallis extracted parameter  $T$  and  $q$  for  $D^0$  ( $\Lambda_c^+$ ) with pseudorapidity by considering both color reconnection mode on and off.

ble II. This is because the contribution of collective radial flow increases with charged-particle multiplicity as found in Ref. [24]. It is also observed that the value of kinetic freeze-out temperature decreases with particle multiplicity, which matches with the previous findings [24].

Further, to have a complete picture, we have extended this analysis to study  $T_{kfo}$  as a function of  $p_T$  and  $\eta$  using the same linear equation given in Eq. 14. It is observed that particles having high- $p_T$  values have higher values of  $T_{kfo}$ . The value of kinetic freeze-out temperature for high-multiplicity classes and high- $p_T$  range ( $8.0 < p_T < 8.8$ ) GeV/c is  $T_{kfo} = 0.164 \pm 0.024$  GeV, whereas for low- $p_T$  range ( $0.2 < p_T < 0.6$ ) GeV/c,  $T_{kfo} = 0.050 \pm 0.009$  GeV. This is possible because the radial flow contribution decreases with  $p_T$  as observed in literature [45]. It is an interesting observation, as it gives an idea of the survivability of the particle carrying high momentum in the thermalized medium. Jets are mostly associated with high- $p_T$ . This observation gives an idea of the interplay of processes initiated by hard-QCD and soft-QCD processes. In the case of pseudorapidity dependence, we observed that the particles at midrapidity have a high value of  $T_{kfo}$ , and it decreases towards the forward rapidity region. The value of kinetic freeze-out

temperature in the rapidity range ( $0.0 < \eta < 0.2$ ) is  $T_{kfo} = 0.165 \pm 0.070$  GeV and it decreases rapidly towards higher rapidities. The discussed results are shown in fig.8 of the appendix.

### C. Correlation between various quantities

The medium formed in the hadronic or nucleus-nucleus collisions at the ultra-relativistic energies is very complex in nature. It involves the interplay of various processes like underlying events, MPIs, rescattering, etc. Some processes are significant in the partonic phase, while others dominate in the hadronic phase. It is possible to expect some reminiscence of partonic level effects in the hadron gas. With this motivation, in this section, we discuss the correlation between Tsallis effective temperature and non-extensive parameter as a function of charged-particle multiplicity and inverse of Knudsen number with the number of multi-partonic interactions ( $n_{MPI}$ ). For simplicity, we call the inverse of the Knudsen number as inverse  $K_n$  now onwards.

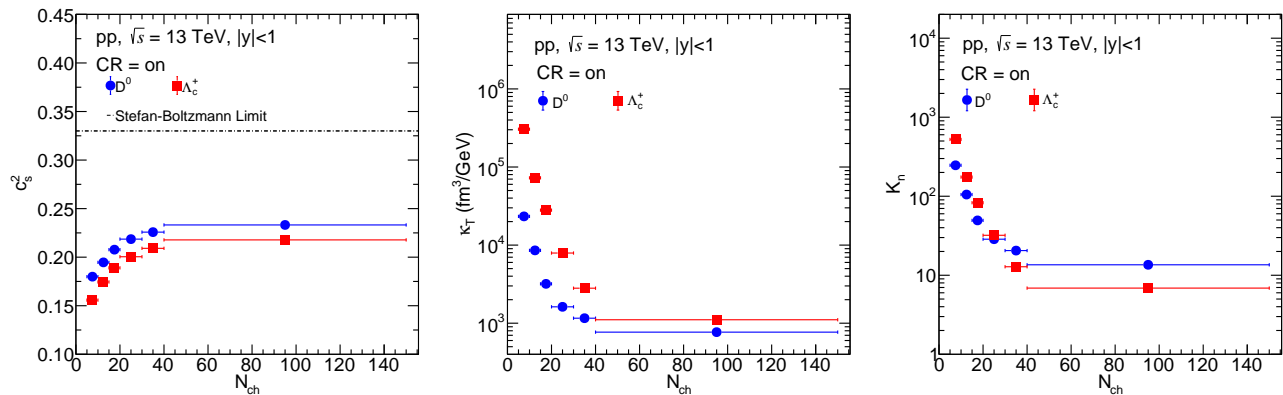


FIG. 6: (Color online) Thermodynamic quantities like, the squared speed of sound square ( $c_s^2$ ) (left), isothermal compressibility ( $\kappa_T$ ) (middle), Knudsen number ( $K_n$ ) (right), with charged-particle multiplicity.

### 1. Correlation between Tsallis parameters

In section III A, we observed that the Tsallis effective temperature ( $T$ ) is related to the non-extensive parameter ( $q$ ). Further, it is observed that the  $q$  values deviate from unity in the case of a system following Tsallis-Boltzmann distribution. This may indicate the presence of long-range correlations, temperature fluctuation, and finiteness of the system. However, in Ref. [12], it is observed that the finite size effect alone cannot explain the appearance of a deviation from  $q = 1$ , which suggests the presence of correlations in the QCD medium plays a vital role in the onset of non-extensivity. Here, we explicitly observe the interplay of fluctuation in  $T$  with the  $q$ -parameter as a function of charged-particle multiplicity. We have extracted various values of  $T$  and  $q$  for each multiplicity bin by choosing different  $p_T$  ranges and obtained the correlation between them by using the following relation:

$$r(T, q) = \frac{\text{Cov}(T, q)}{\sigma_T \sigma_q}, \quad (15)$$

where  $\sigma_T$  is the standard deviation corresponding to  $T$  and  $\sigma_q$  is the standard deviation corresponding to  $q$ .  $\text{Cov}(T, q)$  is the covariance of  $T$  and  $q$ .  $r(T, q)$  denotes the correlation coefficient.

The left side of Fig. 7 shows the correlation between  $T$  and  $q$  as a function of charged-particle multiplicity. It is observed that the correlation between  $T$  and  $q$  is negative, which means  $T$  and  $q$  are anti-correlated with each other. An increase in the  $T$  value decreases the  $q$  value and vice-versa. This anti-correlation is maintained for all the multiplicity classes. At the lowest multiplicity,  $T$  and  $q$  are perfectly anti-correlated, and this correlation decreases towards higher multiplicities. This implies that as the system moves away from equilibrium, the temperature of the system drops down and vice-versa.

### 2. Correlation between $\frac{1}{K_n}$ and $n_{\text{MPI}}$

$n_{\text{MPI}}$  gives information about the number of multi-partonic interactions for a given impact parameter in a given collision. If the number of multi-partonic interactions is relatively more, the system tends toward thermal equilibrium. Similar observation can be drawn from the inverse  $K_n$ . A large value of the inverse  $K_n$  indicates that the system is more thermal in nature, as evident from Fig. 6. Here, we tried to explore the existence of any correlation between these two quantities and how this correlation behaves for a heavy-flavor baryon and meson. From section III B, we found the information about the variation of the inverse  $K_n$  with charged-particle multiplicity. MC model PYTHIA8 provides information about the  $n_{\text{MPI}}$  in each multiplicity class. With the knowledge of both these quantities with charged-particle multiplicity, we have obtained the correlation between the inverse  $K_n$  and  $n_{\text{MPI}}$  as shown on the right side of Fig. 7. It is observed that there is a perfect correlation between the inverse  $K_n$  with  $n_{\text{MPI}}$  for  $D^0$ . However, such a correlation seems to break for  $\Lambda_c^+$ . This implies that the number of parton-parton interactions varies differently for a baryon as compared to a meson because of their different quark constituents. That means the meson carries the initial state information more accurately as compared to the baryon, because of a nice linear behavior with  $n_{\text{MPI}}$ . It is an interesting observation that needs to be explored further to draw a better conclusion on the production dynamics of heavy-flavored baryons and mesons, and baryons and mesons, in general.

## IV. SUMMARY

In this work, we have studied the heavy-flavored hadrons, namely  $\Lambda_c^+$  and  $D^0$  production dynamics using pQCD inspired model called PYTHIA8 in pp collisions at  $\sqrt{s} = 13$  TeV. The important observations of this paper

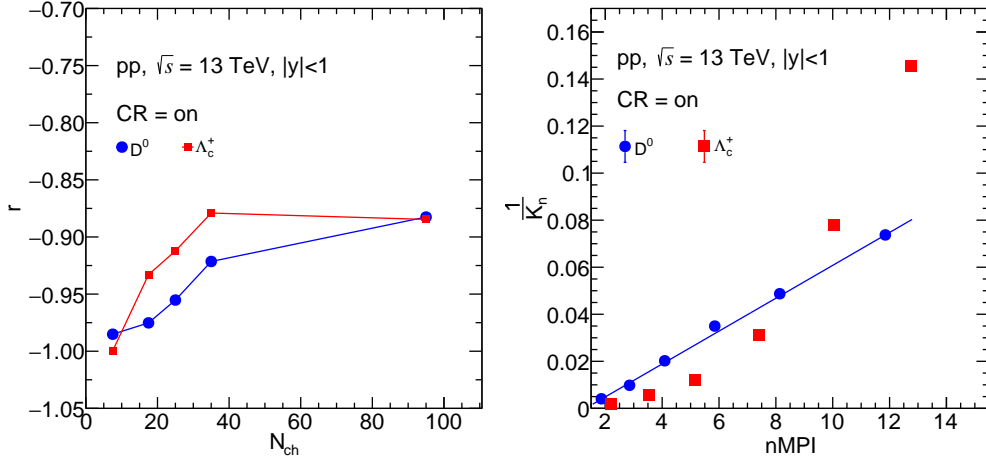


FIG. 7: (Color online) Correlation between (left) Tsallis parameters as a function of charged-particle multiplicity and (right) inverse Knudsen number and  $nMPI$ .

are summarized below.

1. The transverse momentum spectra of  $\Lambda_c^+$  and  $D^0$  produced in pp collision at the center of mass energy  $\sqrt{s} = 13$  TeV are studied using simulated data followed by fitted with the Tsallis distribution function up to  $p_T = 9$  GeV/c. The effect of color reconnection on particle production is clearly observed.
2. The variation of effective temperature and non-extensive parameter ( $q$ ) for  $\Lambda_c^+$  and  $D^0$ , extracted from Tsallis distribution function is studied with charge particle multiplicity ( $N_{ch}$ ), pseudorapidity ( $\eta$ ) and transverse momentum spectra ( $p_T$ ).
3. It is found that for heavy-flavored hadrons, both the effective temperature and non-extensive parameter increase with charged-particle multiplicity. However, the effective temperature decreases with  $p_T$  for low-multiplicity classes and increases with  $p_T$  for high-multiplicity classes. On the other hand, the non-extensive parameter increases at low- $p_T$  and then saturates towards high- $p_T$  for both low and high-multiplicity classes. However, for the high-multiplicity classes, there is a considerable fluctuation in the saturation behavior. The effective temperature decreases and non-extensive parameter,  $q$  increases while going from midrapidity to the forward rapidity region both for  $\Lambda_c^+$  and  $D^0$ .
4. To explore the possible thermal behavior of the produced system, the speed of sound, isothermal compressibility, and the Knudsen number are studied as a function of charged-particle multiplicity. It is observed that at high-multiplicity, the system behaves relatively more like a thermalized medium. Taking the highest multiplicity class of events, we further study the kinetic freeze-out scenario with

different transverse momenta, particle multiplicity, and pseudorapidity.

5. It is found that the kinetic freeze-out temperature decreases with charged-particle multiplicity and the plausible cause for this is the increase in the contribution of radial flow with multiplicity. The kinetic freeze-out temperature was also found to increase with  $p_T$ . As expected, the low- $p_T$  region is found to be more thermalized as compared to the high- $p_T$  region because of the dominance of pQCD-based processes producing more number of jets and mini-jets. The kinetic freeze-out temperature decreases while going from mid to forward rapidity.
6. We have observed an anti-correlation relation between Tsallis Parameters viz.,  $T$  and  $q$  with charged-particle multiplicity. Additionally, we observe a strong correlation between the inverse of the Knudsen number and the number of multi-partonic interactions for meson. The correlation seems to break for heavy-flavored baryon. This needs further investigation to see any possible baryon-meson effect at the partonic level activities in the process of particle production.

## ACKNOWLEDGEMENT

BS acknowledges the doctoral fellowship from CSIR, Government of India. The authors gratefully acknowledge the DAE-DST, Govt. of India funding under the mega-science project – “Indian participation in the ALICE experiment at CERN” bearing Project No. SR/MF/PS-02/2021-IITI (E-37123). The usage of ALICE Tier-3 computing facility at IIT Indore is gratefully acknowledged.

- 
- [1] J. Adam et al. [ALICE Collaboration], *Nature Phys.* **13**, 535 (2017).
- [2] W. Li [CMS Collaboration], *J. Phys. G* **38**, 124027 (2011).
- [3] V. Khachatryan et al. [CMS Collaboration], *JHEP* **09**, 091 (2010).
- [4] A. N. Mishra, G. Paic, C. Pajares, R. P. Scharenberg and B. K. Srivastava, *Eur. Phys. J. A* **57**, 245 (2021).
- [5] S. Deb, S. Tripathy, G. Sarwar, R. Sahoo and J. e. Alam, *Eur. Phys. J. A* **56**, 252 (2020).
- [6] E. G. Ferreira and C. Pajares, *Phys. Rev. C* **86**, 034903 (2012).
- [7] B. Z. Kopeliovich, H. J. Pirner, I. K. Potashnikova, K. Reygers and I. Schmidt, *Phys. Rev. D* **88**, 116002 (2013).
- [8] S. Deb, D. Thakur, S. De and R. Sahoo, *Eur. Phys. J. A* **56**, 134 (2020).
- [9] B. Abelev *et al.* [ALICE], *Phys. Lett. B* **712**, 165 (2012).
- [10] D. Adamová *et al.* [ALICE], *Phys. Lett. B* **776**, 91 (2018).
- [11] A. Ortiz Velasquez, P. Christiansen, E. Cuautle Flores, I. Maldonado Cervantes, G. Paic, *Phys. Rev. Lett.* **111**, 042001 (2013).
- [12] S. Deb, G. Sarwar, R. Sahoo and J. e. Alam, *Eur. Phys. J. A* **57**, 195 (2021).
- [13] S. Deb, S. Tripathy, G. Sarwar, R. Sahoo and J. e. Alam, *Eur. Phys. J. A* **56**, 252 (2020).
- [14] L.D. Landau, *Izv. Akad. Nauk. SSSR* **17**, 51 (1953).
- [15] S. Belenkij, L.D. Landau, *Usp. Fiz. Nauk.* **56**, 309 (1955).
- [16] S. Belenkij, L.D. Landau, *Nuovo Cimento Suppl.* **3**, 15 (1956).
- [17] D. ter Haar (Ed.), *Collected papers of L.D. Landau*, Gordon & Breach, New York, p. 665 (1965).
- [18] J. Cleymans and D. Worku, *J. Phys. G* **39**, 025006 (2012).
- [19] J. Cleymans and D. Worku, *Eur. Phys. J. A* **48**, 160 (2012).
- [20] C. Y. Wong and G. Wilk, *Phys. Rev. D* **87**, 114007 (2013).
- [21] A. Khuntia, H. Sharma, S. Kumar Tiwari, R. Sahoo and J. Cleymans, *Eur. Phys. J. A* **55**, 3 (2019).
- [22] C. Tsallis, *J. Stat. Phys.* **52**, 479 (1988).
- [23] T. Bhattacharyya, J. Cleymans, A. Khuntia, P. Pareek and R. Sahoo, *Eur. Phys. J. A* **52**, 30 (2016).
- [24] P. Ghosh, S. Muhuri, J. K. Nayak and R. Varma, *J. Phys. G* **41**, 035106 (2014).
- [25] R. N. Patra, B. Mohanty and T. K. Nayak, *Eur. Phys. J. Plus* **136**, 702 (2021).
- [26] R. Rath, A. Khuntia, R. Sahoo and J. Cleymans, *J. Phys. G* **47**, 055111 (2020).
- [27] G. Wilk and Z. Wlodarczyk, *Eur. Phys. J. A* **48**, 161 (2012).
- [28] Z. W. Lin, C. M. Ko, B. A. Li, B. Zhang and S. Pal, *Phys. Rev. C* **72**, 064901 (2005).
- [29] T. Pierog, I. Karpenko, J. M. Katzy, E. Yatsenko and K. Werner, *Phys. Rev. C* **92**, 034906 (2015).
- [30] T. Sjostrand, S. Mrenna and P. Z. Skands, *JHEP* **0605**, 026 (2006).
- [31] R. Corke and T. Sjostrand, *JHEP* **03**, 032 (2011).
- [32] Pythia8 online manual: (<https://pythia.org/manuals/pythia8235/Welcome.html>).
- [33] H. S. Shao, *Comput. Phys. Commun.* **184**, 2562 (2013).
- [34] W. E. Caswell and G. P. Lepage, *Phys. Lett. B* **167**, 437 (1986).
- [35] G. T. Bodwin, E. Braaten and G. P. Lepage, *Phys. Rev. D* **51**, 1125 (1995).
- [36] S. Acharya et al. [ALICE Collaboration], *JHEP* **04**, 108 (2018).
- [37] J. Hamon [ALICE Collaboration], *Nucl. Part. Phys. Proc.* **294**, 32 (2018).
- [38] S. Deb, R. Sahoo, D. Thakur, S. Tripathy and A. Khuntia, *J. Phys. G* **48**, 095104 (2021).
- [39] C. Michael and L. Vanryckeghem, *J. Phys. G* **3** L151 (1977).
- [40] C. Michael, *Prog. Part. Nucl. Phys.* **2**, 1 (1979).
- [41] G. Arnison et al. (UA1 Collaboration), *Phys. Lett. B* **118**, 167 (1982).
- [42] R. Hagedorn, *Riv. Nuovo Cim.* **6N10**, 1 (1983).
- [43] M. Ajaz, A. A. K. Haj Ismail, M. Waqas, M. Suleymanov, A. AbdelKader and R. Suleymanov, *Sci. Rep.* **12**, 8142 (2022).
- [44] D. Sahu, S. Tripathy, R. Sahoo and A. R. Dash, *Eur. Phys. J. A* **56**, 187 (2020).
- [45] G. Biró, G. G. Barnaföldi and T. S. Biró, *J. Phys. G* **47**, 105002 (2020).

## Appendix

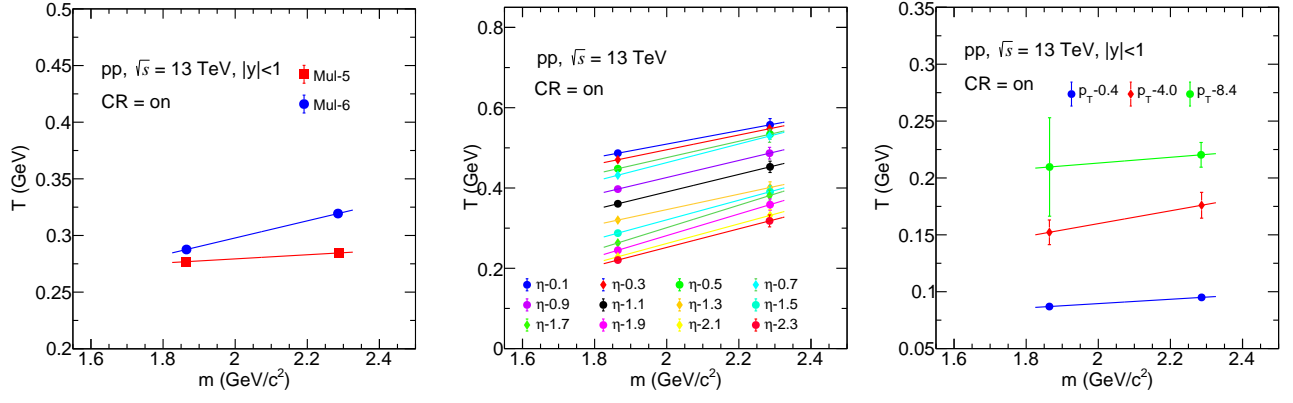


FIG. 8: (Color online) The effective temperature,  $T$  as a function of particle mass for charged-particle multiplicity (left), pseudorapidity (middle), and transverse momentum (right).